Supplementary Materials to "A Railway Accident Prevention System Using An Intelligent Pilot Vehicle"

Shixiong Wang, Xinke Li, Zhirui Chen, and Yang Liu

Appendix A
Another Formulation for Generating x_{ref}

In the main body of the paper, we study the formulation that minimizes the total jerk, i.e., the integral $\int_0^T \frac{1}{m}\left|\frac{du(t)}{dt}\right| dt$. To be specific, we study

$$\min_{u(t)} p_m^c - p_m^b + \lambda_1 \int_0^T |u(t)\cdot v(t)|\, dt + \lambda_2 \int_0^T \frac{1}{m}\left|\frac{du(t)}{dt}\right| dt \tag{1}$$

Subject to

$$\frac{dp_m}{dt} = v_m, \tag{2}$$
$$\frac{dx_{ref}}{dt} = v - v_m, \tag{3}$$
$$\frac{dv}{dt} = \epsilon\frac{u}{m} - c_0 - c_1 v - c_2 v^2 - g\sin\theta - g\frac{700}{\rho}, \tag{4}$$
$$x_{ref}|_{0\le p_m\le p_m^s} = x_0, v|_{0\le p_m\le p_m^s} = v_m, \tag{5}$$
$$x_{ref}|_{p_m^e\le p_m\le R} = x_0, v|_{p_m^e\le p_m\le R} = v_m, \tag{6}$$
$$x_{ref}|_{p_m^c\le p_m\le p_m^b} = x_{max}, v|_{p_m^c\le p_m\le p_m^b} = v_m, \tag{7}$$
$$p_m^s \le p_m^c \le p_m^b \le p_m^e, \tag{8}$$
$$v - v_m \le v_{max}^{\Delta}, \tag{9}$$
$$-\underline{U} \le u \le \overline{U}, u \in \mathbb{C}^0[0,T], \tag{10}$$

In this appendix, as a supplementary discussion, we study an alternative formulation, i.e., we minimize the worst-case jerk. To be specific, we investigate

$$\min_{u(t)} p_m^c - p_m^b + \lambda_1 \int_0^T |u(t)\cdot v(t)|\, dt + \lambda_2 \max_{0\le t\le T} \frac{1}{m}\left|\frac{du(t)}{dt}\right|, \tag{11}$$

subject to (2)∼(10). By introducing an auxiliary variable γ, the worst-case (i.e., min-max) jerk formulation is equivalent to

$$\min_{u(t),\gamma} p_m^c - p_m^b + \lambda_1 \int_0^T |u(t)\cdot v(t)|\, dt + \lambda_2\gamma, \tag{12}$$

subject to

$$\max_{0\le t\le T} \frac{1}{m}\left|\frac{du(t)}{dt}\right| \le \gamma \tag{13}$$
$$\text{Eqs. } (2)\sim(10). \tag{14}$$

That is,

$$\min_{u(t),\gamma} p_m^c - p_m^b + \lambda_1 \int_0^T |u(t)\cdot v(t)|\, dt + \lambda_2\gamma, \tag{15}$$

subject to

$$\frac{1}{m}\left|\frac{du(t)}{dt}\right| \le \gamma, \quad \forall t\in[0,T] \tag{16}$$
$$\text{Eqs. } (2)\sim(10). \tag{17}$$

As explained in the main body of the paper, for technical convenience in problem-solving, we replace the absolute function with the quadratic function. We have

$$\min_{u(t),\gamma} p_m^c - p_m^b + \lambda_1 \int_0^T \left[u(t) \cdot v(t)\right]^2 dt + \lambda_2 \gamma, \tag{18}$$

subject to

$$\frac{1}{m}\left(\frac{du(t)}{dt}\right)^2 \leq \gamma, \quad \forall t \in [0, T] \tag{19}$$

$$\text{Eqs. } (2) \sim (10). \tag{20}$$

With keeping all the shared parameters (e.g., λ_1, λ_2, etc.) in the experiments the same as those in the total jerk case, the experimental results of this min-max jerk formulation are given in Fig. 1. As we can see, in the min-max jerk case, the generated optimal control $u(t)$ is no longer smooth, which is not a desired property. In contrast, in the total jerk case, the generated optimal control $u(t)$ is smooth; see Fig. 9 (b) and (f) in the main body of the paper.

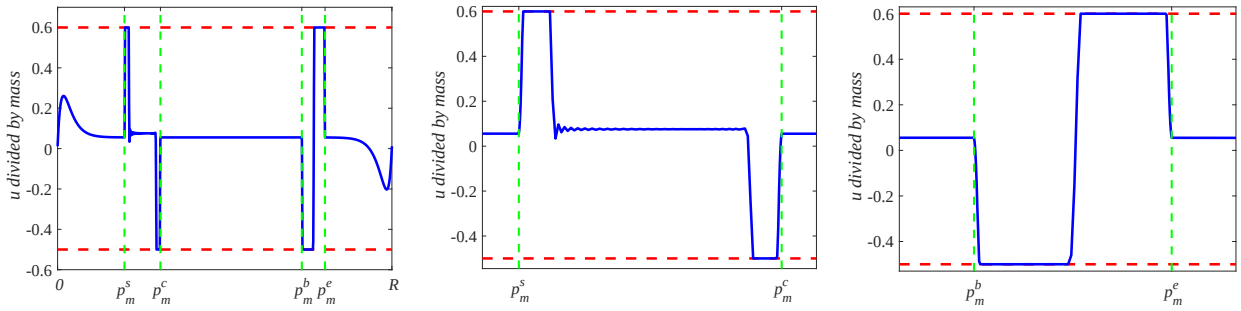

(a) u divided by mass (b) Closeup of (a) (c) Closeup of (a)

Fig. 1. Optimal u generated by the min-max formulation; cf. Fig. 9 (b) and (f) in the main body of the paper.

Remark 1: We may also suppose that the real-time jerk function is upper-bounded. That is, we may solve

$$\min_{u(t)} p_m^c - p_m^b + \lambda_1 \int_0^T \left|u(t) \cdot v(t)\right| dt, \tag{21}$$

subject to

$$\frac{1}{m}\left|\frac{du(t)}{dt}\right| \leq \theta, \quad \forall t \in [0, T] \tag{22}$$

$$\text{Eqs. } (2) \sim (10). \tag{23}$$

where $\theta \geq 0$ is the specified upper bound of the absolute value of the jerk function. Compared to the min-max jerk case, the upper bound θ in this bounded jerk case is fixed and not expected to be minimized. This bounded-jerk formulation should be used when practitioners are confident about their knowledge of the upper bound θ. However, in terms of the smoothness of the control $u(t)$, there exists no difference between this bounded-jerk formulation and the discussed min-max jerk formulation: Both cannot guarantee the smoothness of the control $u(t)$. □

APPENDIX B
DISCUSSION ON REGENERATIVE BRAKING

There are several practical reasons why we did not consider regenerative braking technology for pilot vehicles.

1) First, it is true that "regenerative braking" and "automatic train operation" are mature technologies for trains [1], [2], but only for trains running in urban rail lines (i.e., metro, subway, underground system, etc.); they are not widely implemented technologies in main lines and high-speed lines [1], [3]–[8]. Note that the urban rail lines are enclosed systems, but the main lines and high-speed lines are open systems [1]. It means that the urban rail lines work in a relatively safe environment and the proposed pilot-vehicle-based accident prevention mechanism is not really necessary. Instead, as this paper claimed, we design the pilot-vehicle-based accident prevention mechanism mainly for main-line railways and high-speed railways that lie in a relatively open and diverse environment, e.g., the existence of possible mudslides and landslides, the existence of massive maintenance workers, the possibility to be trespassed by passengers, etc. In contrast, such potential dangers are rarely seen in urban rail lines: to be specific, note that urban rail lines are not in mountainous areas so that mudslides and landslides are scarce; note also that urban rail lines are greatly enclosed so that passengers are not easy to trespass.

2) Second, in regenerative braking, a large energy storage device is required to store energies generated by the braking process. However, according to [1, p. 568],

   "due to the high expense and limited capacity of energy storage devices, most trains in real-world applications are currently not equipped with these devices."

   This claim can also be found in online resources such as https://energyeducation.ca/encyclopedia/Regenerative_braking.
3) Third, due to the maximum charging rate of the energy storage mechanisms, the braking force from a regenerative braking system (RBS) is limited. Therefore, a traditional friction brake system is still required to maintain the safe operation of a vehicle when heavy braking is necessary. Note that for a pilot vehicle, we need to reduce the deceleration distance so that most of the time, the relative distance between the mother train and the pilot vehicle is sufficiently large (i.e., the pilot vehicle can reliably provide warnings for its mother train). As a result, a heavy braking capacity is necessary for the pilot vehicle, and therefore, the regenerative braking system is not sufficient.
4) Fourth, the mass of a pilot vehicle is significantly small compared to a train that includes a locomotive and several carriages. That means the kinetic energy of a pilot vehicle is relatively small, and therefore, the kinetic energy wasted is greatly limited. On the other hand, not every train is deployed with a pilot vehicle. Also, a train is not always associated with a pilot vehicle in its service life. As this paper claims, a train uses a pilot vehicle ONLY when it runs in mountainous areas during rainy days. As such, the kinetic energy wasted is further limited.
5) Fifth, deploying the extra equipment (i.e., the regenerative braking system) on the pilot vehicle means the extra significant mass, which, on the contrary, improves the energy consumption in the acceleration and cruise stages. Hence, there exists a trade-off between the amount of saved energy and the amount of extra consumed energy; for more information, see https://energyeducation.ca/encyclopedia/Regenerative_braking. As such, we leave the issue (of whether to deploy the regenerative braking system on the pilot vehicle) to practitioners who implement the proposed accident prevention mechanism.
6) Sixth, the main focus of this paper is to design the pilot-vehicle-based accident prevention scheme. Other detailed and advanced technologies in implementation deserve independent scientific research or engineering practice.

APPENDIX C
DERIVATION OF PID CONTROLLER

Since the x_{ref} tracking problem is not a high-accuracy-required application, a properly designed PID controller is sometimes sufficient to utilize in practice. The PID controller is given as

$$u_{ref}(t) = Pe(t) + I\int_0^t e(t)dt + D\frac{de(t)}{dt}, \tag{24}$$

where P, I, and D are designed controller parameters. Therefore, incorporating (24) into the system dynamics of the pilot vehicle, the whole system dynamics becomes

$$\begin{cases} \dfrac{dp_m}{dt} &= v_m \\ \dfrac{dx}{dt} &= v - v_m \\ \dfrac{dv}{dt} &= \epsilon\dfrac{u_{ref}}{m} - c_0 - c_1 v - c_2 v^2 - g\sin\theta - g\dfrac{700}{\rho} \\ \dfrac{du_{ref}}{dt} &= P\dfrac{d(x_{ref}-x)}{dt} + I(x_{ref}-x) + D\dfrac{d^2(x_{ref}-x)}{dt^2}, \end{cases} \tag{25}$$

with initial conditions $p_m|_{t=0} = 0$, $x|_{t=0} = x_0$, $v|_{t=0} = v_m|_{t=0} = 0$ and $u_{ref}|_{t=0} = 0$. In (25), $v_m(t)$ and $x(t)$ are obtained from the corresponding sensing devices and fed to the controller directly. Recall that x_{ref} is directly a function of p_m (see Subsection III-C in the main body of the paper) and indirectly a function of the time t.

Eq. (25) in the present form is not a standard form of ordinary differential equations (ODEs) because time derivatives are involved in the right-hand-side of the ordinary differential equation du_{ref}/dt. Besides, we do not know the values of dx_{ref}/dt and d^2x_{ref}/dt^2. For a real application, it does not matter since we can use (24) to generate control signal $u_{ref}(t)$ directly. However, for the simulation study in this paper, we need to transform it into a standard one so that we can invoke standard ODEs solvers, e.g., Runge–Kutta methods. Since

$$\frac{dx_{ref}}{dt} = \frac{dx_{ref}}{dp_m}\cdot\frac{dp_m}{dt} = v_m\cdot\frac{dx_{ref}}{dp_m}, \tag{26}$$

$$\frac{d^2x}{dt^2} = \frac{d(\frac{dx}{dt})}{dt} = \frac{dv}{dt} - \frac{dv_m}{dt} = \frac{dv}{dt} - v_m\cdot\frac{dv_m}{dp_m}, \tag{27}$$

and

$$\frac{d^2x_{ref}}{dt^2} = \frac{d(\frac{dx_{ref}}{dt})}{dt} = \frac{d(v_m \cdot \frac{dx_{ref}}{dp_m})}{dp_m} \cdot v_m = v_m \cdot \frac{dv_m}{dp_m} \cdot \frac{dx_{ref}}{dp_m} + v_m^2 \cdot \frac{d^2x_{ref}}{dp_m^2}, \tag{28}$$

we have

$$\frac{du_{ref}}{dt} = P\left[v_m \cdot \frac{dx_{ref}}{dp_m} - \frac{dx}{dt}\right] + I\left[x_{ref} - x\right] + D\left[v_m \cdot \frac{dv_m}{dp_m}\frac{dx_{ref}}{dp_m} + v_m^2 \cdot \frac{d^2x_{ref}}{dp_m^2} - \frac{dv}{dt} + v_m \cdot \frac{dv_m}{dp_m}\right]. \tag{29}$$

Eq. (29) transforms (25) into a standard form of ODEs which could be solved by standard solvers. Note that the values of dx/dt and dv/dt are available from (25) and x and v_m are from sensing devices. Note also that x_{ref}, dx_{ref}/dp_m, dv_m/dp_m, and d^2x_{ref}/dp_m^2 are available from the design procedure (see Subsection III-C in the main body of the paper).

APPENDIX D
FEASIBILITY ANALYSIS OF VISION-BASED TRACK INSPECTION SYSTEM

Due to the prohibitively high costs and insurmountable constraints, it is intractable for us to validate the feasibility of our visual railway inspection system through real-world deployment. Nevertheless, we still provide a mathematical model analysis incorporating realistic parameters in the following content. The analysis starts by imaging system analysis based on imaging distance and quality, followed by

A. Imaging System

Imaging Distance. We define two distances related to the track inspection system. Lens working distance d_w: the distance between the front surface of the lens and the nearest point of the object being imaged that is in focus. Emergency Braking Distance d_p: the distance that a train experiences when it brakes itself with its highest braking efforts. To make sure that the pilot vehicle can react to the inspected anomaly promptly, the distances must follow $d_p \leq d_w$. The calculation of d_p is proposed in Sec. D-B. In practice, we can simply increase the focal length of the camera lens (i.e., zoom in) to obtain a large d_w. A simulated example of zoom-in image is illustrated in Fig. 3. It shows that by adjusting the camera lens carefully, we can obtain a distant view of the railway that is similar to images from the RailSem19 dataset. Moreover, it is not necessary to re-adjust the camera since the pixel location of the rail track will not shift obviously during the operation process, which is demonstrated in Sec. D-C.

Image Quality. We are also concerned with ensuring image quality to enhance the ability of the inspection system. Specifically, in high-speed railway scenarios, image quality is primarily constrained by two factors: depth of field (DOF) and motion blur. The DOF refers to the range of sharpness in a photograph or image, where objects farther or closer than the working distance appear blurred. To calculate the DOF, the near limit (NL), which is the closest distance at which objects appear sharp, and the far limit (FL), which is the furthest distance at which objects appear sharp, must be computed. The NL can be obtained by

$$NL = \frac{d_w f_l^2}{f_l^2 - k_f \delta_c (d_w - f_l)},$$

and FL can be obtained by

$$FL = \frac{d_w f_l^2}{f_l^2 + k_f \delta_c (d_w - f_l)},$$

where f_l is the focal length of the lens, k_f is the aperture (f-number), and δ_c is the circle of confusion, which is the maximum acceptable diameter of a blur circle in the image plane for it to be considered sharp. Suppose a common setting of cameras and lens, which includes $k_f = 2.8$, $d_w = 100\text{m}$, $f_l = 0.3\text{m}$ and $\delta_c = 3.5 \times 10^{-5}\text{m}$, we can obtain 90.18m of NL and 112.21m of FL.

Furthermore, motion blur is a photographic effect that occurs when a moving object is captured over time, resulting in a blurred appearance. To overcome motion blur due to the high speed of the train, we propose using the latest high-speed imaging techniques. Some examples of commercial products of these high-speed cameras are presented in Tab. I. The FPS (frames per second) of a camera greater than 1000 makes it possible to capture clear anomaly images on a high-speed vehicle. In addition, a complementary solution for motion blur is to use a high-intensity strobe light source for exposure [9], which can also be useful for night vision.

TABLE I
EXAMPLES OF HIGH-SPEED IMAGING CAMERAS

Name	Brand	Maximum Resolution (pixels)	Acquisition Speed (FPS)
PHANTOM Miro C320 High-Speed Camera[1]	Darwin Microfluidics	1920 × 1080	1480
SMI-UHS-1024P-05 [2]	SmartMoreInside	2048 × 1024	2000
Falcon4-CLHS M2240[3]	Teledyne DALSA	2240 × 1248	1200

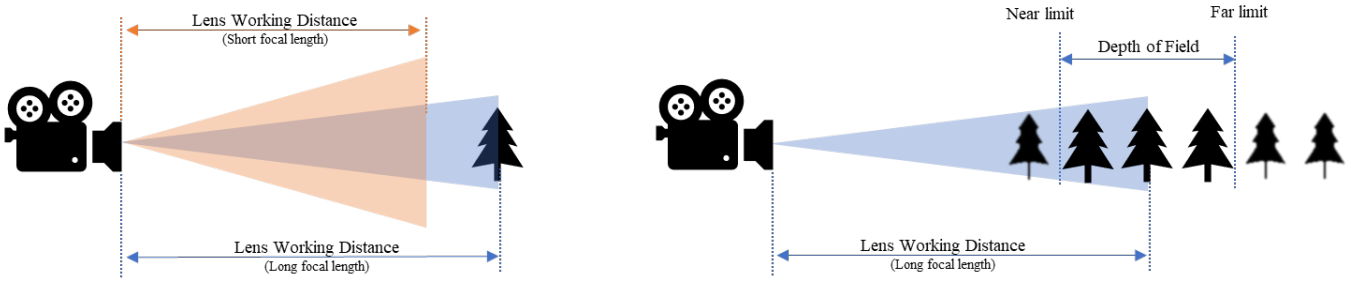

Fig. 2. Visualization of the concepts in the imaging system including lens working distance, depth of field, near limit, and far limit.

Fig. 3. A simulated visualization of increasing the focal length of the camera in a railway scene.

B. Emergency Braking Distance.

Suppose the speed of the pilot (when the pilot sees a rail anomaly) is v, the anomaly identification time of the pilot is t_i (N.B. it takes time to identify an anomaly after seeing it due to vision processing delay), and the emergency braking deceleration of the pilot is b_p. Then, the emergency braking distance of the pilot is

$$d_p = vt_i + v\left(\frac{v}{b_p}\right) - \frac{1}{2}b_p\left(\frac{v}{b_p}\right)^2 = vt_i + \frac{1}{2}\frac{v^2}{b_p}.$$

According to the visual processing results, we have $t_i = 0.1$s. Let $b_p = 3 \times 9.8\text{m/s}^2$ (i.e., three times of gravitational acceleration). Since the mass of a pilot is relatively small and there is no human inside a pilot, a pilot can tolerate a much larger braking deceleration compared to a usual train. Assume $v = 70$m/s (i.e., 250Km/h), which is a high speed in dangerous areas (e.g., mountainous areas during rainy days); see https://en.wikipedia.org/wiki/High-speed_rail. Finally, we have the expected distance $d_p = 88.96$m and have to ensure that $d_w \geq 88.96$m. By implementing the setting of $d_w = 100$m in Appendix D-A, we can obtain a clear imagery view from 90.18m to 112.21m in which interval any value is larger than d_p.

C. Lateral Shift of Track on Image.

It is noted that curved tracks shift laterally from their original vertical alignment on the image. This track shift has the potential to cause the rail tracks to move out of the camera's field of view, making it challenging for anomaly detection. The following content discusses this effect. Consider a curved track as illustrated in Fig. 4. A curved track that has a length of the lens working distance d_w (e.g., segment PC) can be seen as straight. This is because the curvature radius ρ (i.e., the line segment AO) is significantly larger than d_w. Mathematically, the lateral shift of track on d_w location is given by

$$\text{lateral shift DC} = \rho - \sqrt{\rho^2 - \text{PC}^2}$$

To be quantitatively specific, supposing $d_w = 100$m as calculated above and $\rho = 2000$m for a high-speed line (see https://en.wikipedia.org/wiki/Minimum_railway_curve_radius), we have DC $= 2.5$m. By assuming a resolution of 100pixels/m on the bottom horizontal pixels of a 1920×1080 image, which is a typical value in the RailSem19 dataset, the actual track shift

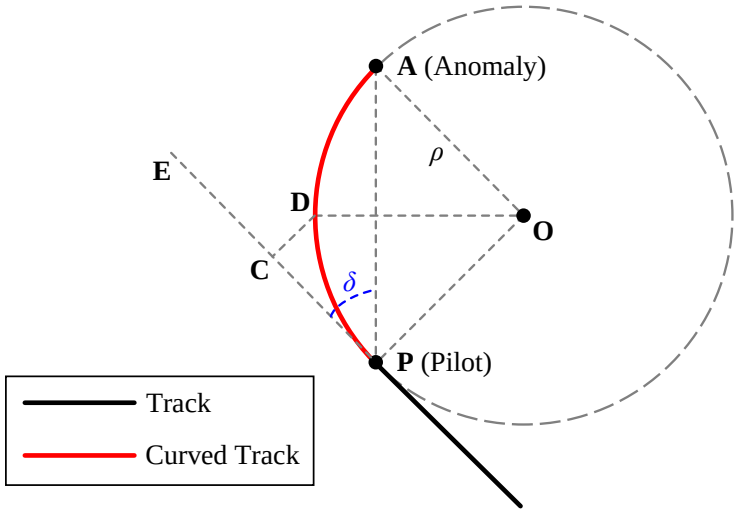

Fig. 4. A short curved track segment (e.g., the arc segment ADP) can be seen as straight since the angle δ of sight is small.

will result in a 250-pixel shift in the image. We note that it is straightforward to ensure that the pixel shift does not cause the rail track to move out of the image by positioning the track in the center of the image.

Furthermore, we consider Δ_d of beginning points tracking in Section IV.D in the main context. Δ_d refers to the maximum pixel distance of beginning points laterally shift between two frames. By assuming the 70m/s of vehicle speed and 0.1s frame processing time, we can obtain the 7m of forward distance for the pilot between two processed frames. Thus, we have $DC = 0.012$m and 1.2-pixel shift based on the above parameter settings. This is a quite small number indicating that the beginning points change is tiny during operation. Finally, we can set Δ_d to be a small number, namely, 10 pixels, for beginning points tracking.

APPENDIX E
MORE RESULTS OF VIDEO-BASED INSPECTION SYSTEM

TABLE II
COMPARISON OF IOU(%) RESULTS ON RAILSEM19 SEMANTIC SEGMENTATION TASK. (C_i IS THE i_{th} CLASS IN RAILSEM19 DATASET.)

Method	C_1	C_2	C_3	C_4	C_5	C_6	C_7	C_8	C_9	C_{10}
SCNN	48.1	52.2	70.2	47.3	46.7	59.4	34.3	29.5	83.9	54.6
FRRNB	50.5	54.0	72.4	40.1	49.8	60.2	36.8	32.5	84.1	59.5
FSCNN	53.4	53.1	71.7	70.2	47.0	62.6	45.6	44.5	84.1	61.9
Method	C_{11}	C_{12}	C_{13}	C_{14}	C_{15}	C_{16}	C_{17}	C_{18}	C_{19}	
SCNN	94.2	45.9	79.5	48.7	18.1	63.9	60.5	68.8	40.3	
FRRNB	94.7	46.7	81.9	50.6	20.7	67.8	62.8	71.5	45.0	
FSCNN	95.8	63.6	89.2	73.1	16.2	72.5	56.7	72.4	54.2	

APPENDIX F
CLOSING NOTES

In this appendix, we provide some closing notes to clear possible confusion from readers.

1) The distances between different adjacent stations are different, leading to different curves of x_{ref}. For this reason, we need to separately design x_{ref} for every two adjacent stations. We just need to plug in the required parameters such as the distance between the two adjacent stations. Then, we can quickly get a specific x_{ref} for the two considered adjacent stations. The computational time of x_{ref} is generally speaking short, just in several seconds; cf. Table II in the experiments in Subsection III-E (title: Experiments). Hence, planning a x_{ref} for every two adjacent stations is computationally easy, which can be done even just before the train is to depart from the starting station.
2) Note that it is the pilot vehicle that dynamically adjusts its relative distance to the mother train. The running plan of the mother train is determined by the Train Scheduling System and is not to be changed by the proposed safety-guaranteeing sub-system. See Remark 4 in the main body of the paper. The x_{ref} is always pre-designed for every two adjacent stations. Hence, during the running of the mother train, the pilot vehicle just uses its power system to generate proper traction and braking forces, and these proper forces allow the real-time relative distance between the train and the pilot to track x_{ref}. In this tracking process, feedback control is necessary, as discussed in Subsection III-D (title: Relative Distance Tracking).

3) As for the moving blocks and/or positive train control issues, they do not influence the design of x_{ref} because the designed x_{ref} is a function of the position p_m of the mother train (cf. Figure 6 in the main body of the paper), NOT a function of the time. To be more specific, when moving blocks and/or positive train control commands require the mother train to stop, the pilot vehicle will also stop because it needs to maintain the distance x_{ref} from the mother train. When the mother train continues running after moving blocks and/or positive train control, the pilot vehicle will also continue running because it needs to maintain the distance x_{ref} from the mother train. This is a benefit of using the feedback control. Note that the stopping/running strategies of the mother train are made by the Train Scheduling System when there exist moving blocks and/or positive train control commands. But this does not influence the running of the pilot vehicle because the pilot vehicle needs to maintain the distance x_{ref} from the mother train. **When the train stops (resp. runs), the pilot also stops (resp. runs).** The only difference is that when the Train Scheduling System makes stopping/running commands for a train due to moving blocks and/or positive train control, the position of the pilot vehicle should also be considered. This is practically easy to implement because we can just treat a train-pilot grouping as a long and multi-unit train. Namely, a pilot vehicle can be seen as a part of a train, e.g., a virtual locomotive.
4) When we design a target distance-speed profile of a mother train (based on moving authority or the service braking curve), we DO NOT consider any emergency situations—we just assume there will NOT exist emergency situations when the train is running according to its pre-designed distance-speed profile. We do not know where the emergency situations will happen along the track, and therefore, it is not practical to design a distance-speed profile for a mother train that takes into consideration of emergency situations. Note that only when we exactly know the positions where the emergency situations happen can we design a so-called target distance-speed profile for braking. Therefore, for the purpose of safety-guaranteeing, the good practice is to use a safe value for the emergency braking distance (i.e., x_s in Figure 6 in the main body of the paper) and let the mother train brake itself as quickly as possible with its highest effort (i.e., using the largest braking force) whenever an emergence is detected.
5) The designed scheme in this paper is more an academic blueprint than a practically validated solution: As a single university, it is difficult for us to make and implement such a pilot vehicle to verify the proposed solution because considerable railroad hardware and facilities are expected to be involved. For example, the cost-benefit analyses of the Positive Train Control (PTC) scheme were conducted by the US government where several universities and companies participated; see Page 12 of the literature

   Peters, J. C., & Frittelli, J. (2018). Positive Train Control (PTC): Overview and Policy Issues.

   Also, to the best knowledge of the authors, neither the authors nor any relevant organizations have conducted specific evaluations for the above candidate solutions—all these solutions are more academic proposals than practical implementations. Therefore, the purpose of this paper is to draw the attention of existing entities (e.g., governments, universities, and companies) to collaborate on testing potential solutions (e.g., the sensor-network-based idea, the drone-based idea, the existing SMART2 idea, the proposed pilot-based idea) to further improve the safety of rail transportation. (For the review of the sensor-network-based idea, the drone-based idea, and the SMART2 idea, see the Introduction.) In other words, we would like to leave detailed, commercial, and financial cost-benefit analyses and verification to our industrial colleagues. We hope that this does not influence the completeness of this paper.
6) We clarify that the situation detection camera must be installed on the pilot vehicle, not the mother train. This is because the effective visual detection distance of a camera is significantly smaller than the emergency braking distance of the mother train. Hence, if the camera is mounted on the mother train and when the railway anomaly (e.g., landslides) is detected by the camera, it is already too late for the mother train to brake itself. In contrast, if the camera is installed on the pilot vehicle and when the railway anomaly is detected by the camera, the mother train has a sufficient buffering distance to brake itself. Note that the relative distance between the pilot vehicle and the mother train is maintained to be larger than the emergency braking distance; see Figure 6 in the main body of the paper. In terms of the pilot vehicle, it has significantly lighter weight than its mother train, which results in a shorter brake distance that can be covered by the range of the visual inspection system. In other words, whenever a railway anomaly is detected by the camera, the pilot vehicle can completely brake itself before reaching the anomaly because it has a small inertia; see also Appendix D.

REFERENCES

[1] J. Yin, T. Tang, L. Yang, J. Xun, Y. Huang, and Z. Gao, "Research and development of automatic train operation for railway transportation systems: A survey," *Transportation Research Part C: Emerging Technologies*, vol. 85, pp. 548–572, 2017.

[2] A. Albrecht, P. Howlett, P. Pudney, X. Vu, and P. Zhou, "The key principles of optimal train control—part 1: Formulation of the model, strategies of optimal type, evolutionary lines, location of optimal switching points," *Transportation Research Part B: Methodological*, vol. 94, pp. 482–508, 2016.

[3] M. Domínguez, A. Fernández-Cardador, A. P. Cucala, and R. R. Pecharromán, "Energy savings in metropolitan railway substations through regenerative energy recovery and optimal design of ato speed profiles," *IEEE Transactions on Automation Science and Engineering*, vol. 9, no. 3, pp. 496–504, 2012.

[4] A. González-Gil, R. Palacin, and P. Batty, "Sustainable urban rail systems: Strategies and technologies for optimal management of regenerative braking energy," *Energy Conversion and Management*, vol. 75, pp. 374–388, 2013.

[5] X. Yang, A. Chen, X. Li, B. Ning, and T. Tang, "An energy-efficient scheduling approach to improve the utilization of regenerative energy for metro systems," *Transportation Research Part C: Emerging Technologies*, vol. 57, pp. 13–29, 2015.

[6] X. Yang, X. Li, B. Ning, and T. Tang, "A survey on energy-efficient train operation for urban rail transit," *IEEE Transactions on Intelligent Transportation Systems*, vol. 17, no. 1, pp. 2–13, 2016.

[7] G. M. Scheepmaker and R. M. Goverde, "Energy-efficient train control using nonlinear bounded regenerative braking," *Transportation Research Part C: Emerging Technologies*, vol. 121, p. 102852, 2020.
[8] W. Zhou, Y. Huang, L. Deng, and J. Qin, "Collaborative optimization of energy-efficient train schedule and train circulation plan for urban rail," *Energy*, vol. 263, p. 125599, 2023.
[9] P. J. Sousa, F. Carneiro, N. V. Ramos, P. J. Tavares, and P. M. Moreira, "Development of led-based illumination system for high-speed digital image correlation," *Procedia Structural Integrity*, vol. 17, pp. 828–834, 2019.